High-Resolution Infrared Study of Vinyl Fluoride in the 750−1050 cm^{-1} Region: Rovibrational Analysis and Resonances Involving the ν_8, ν_{10}, and ν_{11} Fundamentals

Nicola Tasinato,[†] Paolo Stoppa,[†] A. Pietropolli Charmet,[†] Santi Giorgianni,*[,†] and Alberto Gambi[‡]

Università Ca' Foscari di Venezia, DCF, D.D. 2137, I-30123 Venezia, and Università di Udine, DSTC, Via Cotonificio 108, I-33100 Udine, Italy

Received: June 27, 2006; In Final Form: September 27, 2006

The FTIR spectra of CH_2═CHF have been investigated in the ν_8, ν_{10}, and ν_{11} region between 750 and 1050 cm^{-1} at a resolution of about 0.002 cm^{-1}. The ν_8 vibration of symmetry species A′ gives rise to an a/b-type hybrid band, while the ν_{10} and ν_{11} modes of A″ symmetry produce c-type absorptions. Due to the proximity of their band origins, the three vibrations perturb each other by Coriolis and high-order anharmonic resonances. In particular, the interactions between the ν_8 and ν_{10} modes are very strong and widespread with band origins separated by only 1.37 cm^{-1}. Besides the expected c-type characteristics, the ν_{10} band shows a very intense pseudo a-type component caused by the strong first-order Coriolis resonances with the ν_8 state. Furthermore, the $2\nu_9$ "dark state" was found to be involved in the interacting band systems. The spectral analysis resulted in the identification of 3144, 3235, and 3577 transitions of the ν_8, ν_{10}, and ν_{11} vibrations, respectively. Almost all the assigned data were simultaneously fitted using the Watson's A-reduction Hamiltonian in the I^r representation and the perturbation operators. The model employed includes nine types of resonances within the tetrad $\nu_8/\nu_{10}/\nu_{11}/2\nu_9$ and a set of spectroscopic constants for the ν_8, ν_{10}, and ν_{11} fundamentals as well as parameters for the "dark state" $2\nu_9$, and fourteen coupling terms have been determined.

1. Introduction

In the past years, there has been increasing progress in spectroscopic studies of halogenated ethenes motivated, in part, by their potential role as air pollutants in atmospheric chemistry. The considerable interest in the understanding of the rovibrational behavior of vinyl fluoride is mainly based on its importance in atmospheric reactions, since this compound seems to play a significant role in photochemical processes.[1,2]

Vinyl fluoride (fluoroethene) is widely produced by industry and mainly used for the production of synthetic resins such as polyvinyl fluoride. During synthesis and handling, the compound can be accidentally released in the atmosphere, producing severe environmental effects. Moreover, vinyl fluoride, like vinyl chloride and vinyl bromide, is mutagenic and clastogenic and potentially a carcinogenic agent for humans.[3]

Infrared spectroscopy is a very powerful method for detecting trace gases, but in order to profit from the sensitivity of this technique, accurate spectroscopic parameters are required. In particular, the molecular constants obtained from high-resolution spectra are useful not only in quantifying atmospheric pollutants but also to improve theoretical studies dealing with reactivity of haloalkenes toward atmospheric constituents such as ozone and hydroxyl radicals.[4,5]

High-resolution infrared spectra of CH_2═CHF have been widely investigated by this research group, as reported in the references of a recent work.[6] The results obtained led to the determination of accurate molecular parameters for several vibrations and to an understanding of the observed interactions. Very recently, the perturbations affecting the ν_5 and ν_6 normal modes (1280−1400 cm^{-1}) have been explained through a model including six different resonances within the tetrad $\nu_5/\nu_6/\nu_8 + \nu_9/\nu_9 + \nu_{11}$.[6]

Low-resolution infrared studies on this molecule, mainly directed to the identification of the fundamentals, were carried out a long time ago.[7,8] The location of the normal modes ν_8, ν_{10}, and ν_{11} has been a subject of controversy, since the first low-resolution infrared spectrum was published in 1945.[9] The related region around 900 cm^{-1} has been considered by various workers in subsequent investigations[7,10] and satisfactory results were obtained when Coriolis resonances between ν_8, ν_{10}, and ν_{11} bands were considered.[11] Ground-state constants were determined many years ago from microwave spectra[12,13] and more recently using microwave data available in the literature together with infrared combination differences coming from the ν_7 fundamental.[14]

The present work deals with the interpretation of the rovibrational structure of the ν_8, ν_{10}, and ν_{11} bands of vinyl fluoride in the region between 750 and 1050 cm^{-1} where high-resolution spectra have been investigated for the first time. The determination of the spectroscopic parameters of these fundamentals are also of considerable interest, since the related absorptions fall in the range of atmospheric windows for the detection of trace gases. The difficulty concerning the analysis of the ν_8, ν_{10}, and ν_{11} spectral region is mainly due to the very close band origins of ν_8 and ν_{10}, which are separated by only 1.37 cm^{-1}. Furthermore, the three vibrations are affected by different strong resonances which can be understood and treated quantitatively only by employing well-resolved spectra and suitable prediction programs. The complete analysis of the spectra led to the assignment of about 10 000 transitions in the ν_8, ν_{10}, and ν_{11} fundamentals. Besides, the perturbation effects

* To whom correspondence should be addressed. E-mail: giorgian@unive.it.
[†] Università Ca' Foscari di Venezia.
[‡] Università di Udine.

10.1021/jp064013w CCC: $33.50
Published on Web 11/22/2006

TABLE 1: Fundamental Wavenumbers (cm^{-1}) of CH_2═CHF[a]

symmetry species	mode	wavenumber	approximate description
A′	ν_1	3140.0	CH_2 antisym. stretch
A′	ν_2	3093.5	CH stretch
A′	ν_3	3062.1	CH_2 sym. stretch
A′	ν_4	1654.6	C═C stretch
A′	ν_5	1379.5	CH_2 bend
A′	ν_6	1304.5	CH bend
A′	ν_7	1155	CF stretch
A′	ν_8	931.5	CH_2 rock
A′	ν_9	483	C═CF bend
A″	ν_{10}	930.2	CH out of plane bend
A″	ν_{11}	862	CH_2 wag
A″	ν_{12}	711	torsion

[a] From ref 8.

allowed the identification of an additional perturber which was identified as $2\nu_9$ "dark state". Presently, almost all the assigned transitions have been fitted simultaneously from a model which includes nine different resonances within the tetrad $\nu_8/\nu_{10}/\nu_{11}/2\nu_9$.

2. Experimental Details

The sample of CH_2═CHF (purity ≈ 99%) supplied by Peninsular Chemical Research, Inc., was used without further purification. Low-resolution infrared spectra were recorded at room temperature in the range 400−4000 cm^{-1} using the Bruker Vertex 70 spectrometer (at a resolution of 0.2 cm^{-1}) with a 16-cm path cell and pressures in the range 4.5−65 mbar.

The high-resolution spectra were recorded in the region between 750 and 1050 cm^{-1} on the Bruker IFS 120 HR vacuum Fourier transform spectrometer at the University of Giessen, Germany. A globar source, a Ge:KBr beam-splitter, and a Ge:Cu detector were employed. A detailed description of the instrument has been reported elsewhere.[15] The measurements were carried out at room temperature using a 27-cm path cell and a sample pressure of about 1 mbar. The 341 interferograms collected were coadded, apodized with a boxcar function, and Fourier transformed to give a nominal resolution of 0.0019 cm^{-1}. The instrument calibration was performed using suitable CO_2 lines.[16] The wavenumber accuracy for a single measured transition is estimated to be about 3×10^{-5} cm^{-1}.

3. Results and Discussion

Vinyl fluoride is a planar near-prolate asymmetric top ($\kappa = -0.945$) belonging to the C_s symmetry point group. The *a* and *b* principal inertia axes lie in the molecular symmetry plane, while the *c*-axis is perpendicular to it. The molecule has twelve fundamental vibrations (reported in Table 1), of which nine of species A′ ($\nu_1-\nu_9$) give rise to a/b hybrid bands and three of species A″ ($\nu_{10}-\nu_{12}$) produce c-type absorptions.

The ν_8 vibration (~928 cm^{-1}), approximately representing the CH_2-rocking mode, is of symmetry A′, and the transitions follow the usual selection rules for a-type ($\Delta J = 0, \pm1$; $\Delta K_a = 0$; $\Delta K_c = \pm1$) and b-type ($\Delta J = 0, \pm1$; $\Delta K_a = \pm1$; $\Delta K_c = \pm1$) bands. The ν_{10} (~929 cm^{-1}) and ν_{11} (~863 cm^{-1}) modes of symmetry A″ correspond to the out-of-plane CH deformation of the CHF group and to the CH_2-wagging motion, respectively. They give rise to c-type bands with the foremost selection rules ($\Delta J = 0, \pm1$; $\Delta K_a = \pm1$; $\Delta K_c = 0, \pm2$). For all the vibrations, many transitions are expected in the P, Q, and R branches, which will produce several even ($K_a'' + K_c'' = J''$) and odd ($K_a'' + K_c'' = J'' + 1$) subbands.

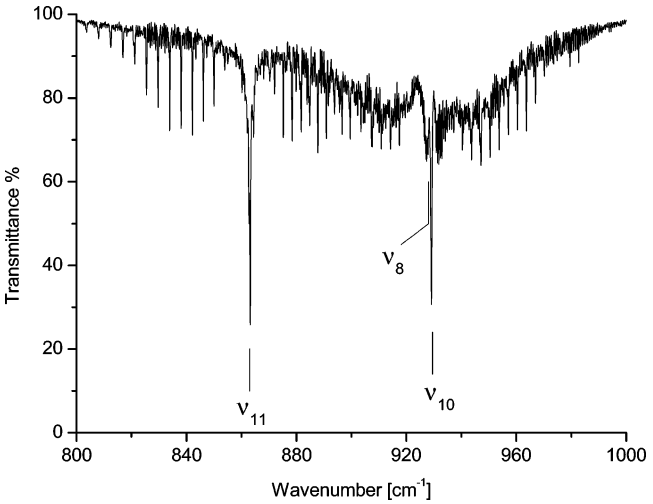

Figure 1. Survey spectrum at low resolution (0.2 cm^{-1}) of vinyl fluoride in the region of the ν_8, ν_{10}, and ν_{11} fundamentals (room temperature, pressure about 4.5 mbar, 16 cm cell).

A low-resolution (0.2 cm^{-1}) survey spectrum of the region investigated is reported in Figure 1 where the ν_{11} and ν_{10} absorptions are clearly visible due to the strong Q branch of these c-type bands, while the ν_8 fundamental is difficult to identify since its a/b-type structure is overlapped by the strong ν_{10} absorption.

3.1. Description and Analysis of the Spectra. *ν_{11} Fundamental.* The investigation of the three band systems started with the analysis of the ν_{11} vibration, as this mode is separated from the ν_8 and ν_{10} fundamentals by about 70 cm^{-1}. As can be observed in Figure 1, only the P-branch transitions are located in a region free of any other absorption. The R-branch lines overlap to a great extent with the P and Q branch features of the ν_8 and ν_{10} modes, giving rise to a spectral structure increasingly dense and of more difficult interpretation.

The structure of a c-type band is mainly dominated by ${}^{P}Q_K$ and ${}^{R}Q_K$ clusters with a separation between neighboring characteristics approximately corresponding to $2(A - \bar{B}) \approx 3.6$ cm^{-1} where $\bar{B} = (B + C)/2$. These clusters, which could be identified for several K_a values, appear as groups of closely spaced lines showing distinct patterns and can be easily assigned since the neighboring features differ by one unit in *J*. The individual ${}^{P}Q_K$ multiplets show the *J* structure resolved for $5 \geq K_a'' \geq 10$, while for $6 \leq K_a'' \leq 9$, the rovibrational details appear more compressed and several transitions are overlapped. The low-resolution spectrum is illustrated in Figure 2, where the ${}^{P}Q_{4-12}$ peaks are indicated. As can be seen from high-resolution spectra, the resolved details in the ${}^{P}Q_{11}$ manifold move to the lower wavenumber side with increasing *J*. The fine structure appears more regular for the ${}^{R}Q_K$ clusters, and the degradation of the resolved lines occurs almost always toward lower wavenumbers. This behavior is also observed in the ${}^{R}Q_0(J)$ manifold up to $J'' = 24$, while for higher *J* values, the degradation develops in the opposite direction. The effect of asymmetry splitting, observed for $K_a' \leq 8$, gives rise to an irregular numbering of the lines, and in the absence of perturbations, the even component is located at higher and lower wavenumber side in the P and R branches, respectively.

The ν_{11} fundamental is essentially unperturbed for levels with $K_a' \leq 7$ except for a few small resonances, which are very localized. Rovibrational levels with $K_a' \geq 8$ are perturbed by different interactions involving ν_8 and ν_{10} states (see later); in

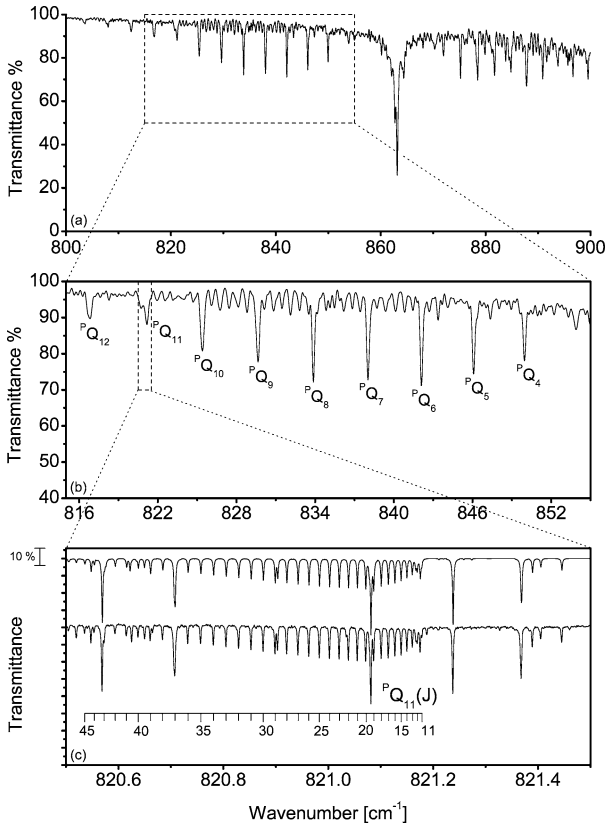

Figure 2. Low-resolution spectrum of the ν_{11} band (a) and identification of the $^{P}Q_{K}$ details (b) (room temperature, pressure about 4.5 mbar, 16 cm cell). (c) A section of the high-resolution spectrum near 821.0 cm^{-1} showing the structure of the $^{P}Q_{11}(J)$ manifold of ν_{11}: upper trace, simulated spectrum; lower trace, observed spectrum ($T = 296$ K, $P \approx 1.0$ mbar, 27 cm cell).

particular, levels with $K_a' = 9$ and 10 are shifted to lower energy, while levels with $K_a' = 8$, 11, 12, and 13 are shifted to higher energy.

The investigation was carried out mainly using an interactive program based on Loomis−Wood-type diagrams. The analysis led to the assignment of 3577 lines in the $^{P}P_{K}$, $^{P,R}Q_{K}$, and $^{R}R_{K}$ subbranches with K_a' ranging from 0 to 17 and $J' \leq 50$.

ν_8 and ν_{10} Fundamentals. Since the ν_8 and ν_{10} vibrations lie very close with band origins separated by only 1.37 cm^{-1}, their rovibrational levels are perturbed for all observed K_a values. The analysis based exclusively on Loomis−Wood correlation diagrams is impractical, in particular for $K_a' \leq 4$, unless a set of molecular parameters including coupling constants is available. The very strong Coriolis resonances shift the spectral lines several reciprocal centimeters, and in some cases, the whole clusters are perturbed. Moreover, the perturbations significantly alter the intensity of the spectral lines and allow transitions which are forbidden by the usual selection rules.

The identification of the $^{R}Q_0$ and $^{P}Q_1$ manifolds of ν_{10} and the assignment of some transitions with $K_a' = 4$ of ν_8 were essential in the analysis of these bands. A preliminary least-squares refinement of the data, including the first-order Coriolis coupling constants, led to the determination of spectroscopic parameters good enough to allow the identification of regular sequences in the Loomis−Wood correlation diagrams and determination of reliable assignments. A spectral portion near the ν_{10} band origin showing the identified details of the $^{R}Q_0$ and $^{P}Q_1$ clusters is depicted in Figure 3.

A very interesting feature in the Q branch spectra of ν_8 and ν_{10} bands is the striking appearance of two sets of clusters $^{Q}Q_{K}$-

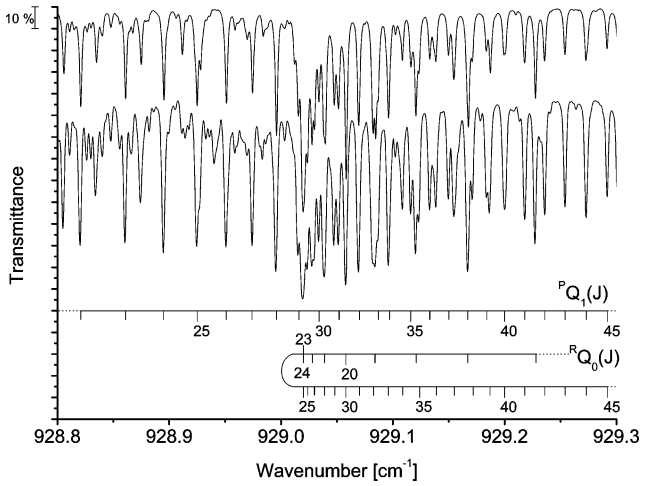

Figure 3. Portion of the CH_2═CHF spectrum (928.8−929.3 cm^{-1}) showing details of $^{P}Q_1(J)$ and $^{R}Q_0(J)$ clusters of the ν_{10} band. Upper trace: simulated spectrum. Lower trace: observed spectrum ($T = 296$ K, $P \approx 1.0$ mbar, 27 cm cell).

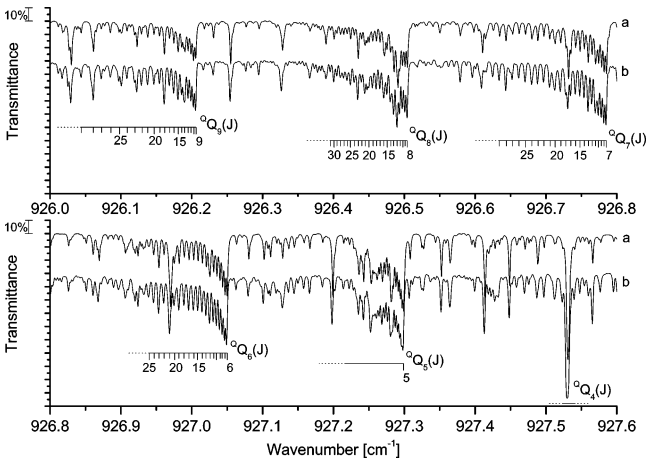

Figure 4. High-resolution spectrum of CH_2═CHF in the region between 926.0 and 927.6 cm^{-1}: $^{Q}Q_9(J) - {}^{Q}Q_6(J)$ manifolds indicate the fine structure of the ν_{10} pseudo a-type component, while the $^{Q}Q_5(J)$ and $^{Q}Q_4(J)$ clusters refer to the ν_8 a-type component (see text). Trace a: simulated spectrum. Trace b: observed spectrum ($T = 296$ K, $P \approx 1.0$ mbar, 27 cm cell).

(J) ($\Delta J = \Delta K_a = 0$) instead of the only one expected for the a-type component of the ν_8 band. The second series of clusters results arising from the pseudo a-type component of the ν_{10} vibration, due to ν_8/ν_{10} strong Coriolis resonances. The involved transitions, which are characterized by $\Delta K_a = \Delta K_c = 0$, are not usual, since the selection rules for a c-type band give rise to lines with $\Delta K_a = \pm 1$ and $\Delta K_c = 0$ or $\Delta K_a = \pm 1$ and $\Delta K_c = \pm 2$, with the former being stronger than the latter. The individual clusters, expected to show the J details resolved as the K_a value increases, display a structure degrading to low-wavenumber side, and the perturbation effects give rise to peculiar patterns. An interesting observation comes from the localization of the ν_8 and ν_{10} $^{Q}Q_{K}(J)$ manifolds reproduced in Figure 4. The series of the $^{Q}Q_{K}$ clusters arising from the a-type and the pseudo a-type component of ν_8 and ν_{10}, respectively, appears as the continuation of each other, and as can be observed, the $^{Q}Q_{4-5}(J)$ peaks derive from ν_8, while the contiguous $^{Q}Q_{6-9}(J)$ groups belong to ν_{10}. A different trend is found in the range 930−939 cm^{-1} still characterized by the presence of the $^{Q}Q_{K}(J)$ clusters of ν_8 and ν_{10} fundamentals. The behavior is analogous to that reproduced in Figure 4, but the assignment is now exactly opposite: the $^{Q}Q_{4-5}(J)$ peaks belong to ν_{10}, while

the contiguous ${}^{Q}Q_{6-17}(J)$ groups derive from ν_8. The shifts in the K_a levels of the ν_8 and ν_{10} states are mainly produced by the first-order a-type Coriolis resonance, and the very strong intensities of the pseudo-parallel transitions emphasize, one more time, the strength of the interactions occurring between the ν_8 and ν_{10} vibrations.

A remarkable number of even and odd transitions ($0 \leq K_a' \leq 11$ and $J' \leq 38$) belonging to the subbranches ${}^{Q}Q_K$, ${}^{Q}P_K$, and ${}^{Q}R_K$ of the pseudo a-type component of ν_{10} were assigned by considering the ground-state combination differences. Besides, some transitions with $\Delta K_a = -2$, $\Delta K_c = +2$, and $\Delta J = -1$ and 0 were also identified. Concerning the expected c-type component of the ν_{10} band, many transitions belonging to the subbranches ${}^{P}P_K$, ${}^{P,R}Q_K$, and ${}^{R}R_K$ were assigned with K_a' ranging from 0 to 17 and $J' \leq 50$.

The ν_8 band shows a predominant a-type component, so that most of the assignments ($0 \leq K_a' \leq 17$ and $J' \leq 50$) involve ${}^{Q}P_K$, ${}^{Q}Q_K$, and ${}^{Q}R_K$ subbranches. Resolved lines for the b-type component could only be identified for transitions with $J' \leq 39$ and $4 \leq K_a' \leq 11$. Some weak lines characterized by $\Delta K_a = \pm 2$ were also assigned.

As a final point, it should be noted that the asymmetry splitting, observed for $K_a' \leq 8$ and 9 in the ν_8 and ν_{10} bands, respectively, makes the structure of the spectra more complicated. The resulting assignments are more difficult, since in some cases, only the even or the odd component is affected by perturbations. The analysis becomes more complicated when both components are involved in different types of interactions, so yielding different shifts and intensities for transitions with the same K_a value.

3.2. Interactions Involving ν_8, ν_{10}, ν_{11}, and $2\nu_9$ States. As pointed out in the subband analyses, the ν_8 and ν_{10} vibrations are strongly perturbed, and the interactions involve all the rovibrational levels. Besides, both vibrations also interact with the ν_{11} normal mode. It is worthwhile to note that, when the ν_8 and ν_{10} transitions with $K_a' = 5$ and 6 are considered, no satisfactory results are obtained even when all the $\nu_8/\nu_{10}/\nu_{11}$ resonances are included in the fit. These anomalies indicate that additional perturbers have to be considered in order to explain all the observed interaction effects. In the range examined, there is no evidence of further absorptions than those coming from the fundamentals, and then the $2\nu_9$ overtone "dark state" should be responsible for further resonances occurring in the range investigated. The reduced energy diagram of ν_8, ν_{10}, and $2\nu_9$ states for low K_a values, obtained from the parameters given in Tables 5 and 6 (see later), is depicted in Figure 5. The employed model to explain the interacting vibrations involving the tetrad $\nu_8/\nu_{10}/\nu_{11}/2\nu_9$ as illustrated in Figure 6, which shows the vibrational energy level diagram in the spectral range investigated and the different resonances occurring among the interacting states.

From symmetry considerations, the A′ and A″ modes may interact through a-type ($\Delta K_a = 0, \pm 2, ...$) as well as b-type ($\Delta K_a = \pm 1, \pm 3, ...$) Coriolis resonance according to the selection rules ($E^{\pm} \leftrightarrow E^{\mp}, O^{\pm} \leftrightarrow O^{\mp}$) and $E^{\pm} \leftrightarrow O^{\pm}$, respectively. On the other hand, vibrations with the same symmetry may interact by c-type Coriolis perturbation ($\Delta K_a = \pm 1, \pm 3, ...$) and/or through anharmonic resonance ($\Delta K_a = 0, \pm 2, ...$) following the selection rules $E^{\pm} \leftrightarrow O^{\mp}$ and ($E^{\pm} \leftrightarrow E^{\pm}$, $O^{\pm} \leftrightarrow O^{\pm}$), respectively.

The band origins of ν_8 and ν_{10} fundamentals are in very close proximity, and the interaction between these two vibrations is the strongest and largest involving all the rovibrational levels. Since the two vibrations have different symmetry, they can interact by both a- and b-type Coriolis resonances. The major effects are caused by first-order perturbations: $\Delta K_a = 0$ and $\Delta K_a = \pm 1$ for a- and b-type Coriolis interactions, respectively. The latter mainly involves the levels with $K_a' \leq 4$, while the a-type Coriolis resonance affects the bands globally. Table 2 summarizes all the observed crossings among the different states, and as can be seen, those involving ν_8 and ν_{10} are due to first-

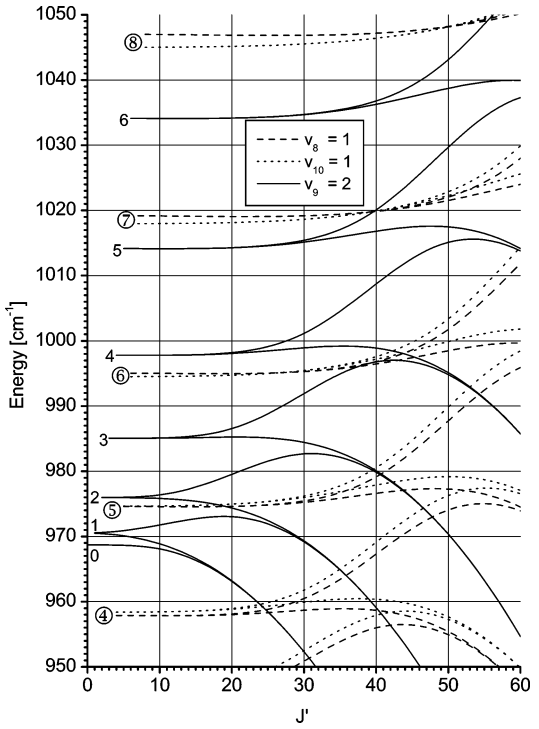

Figure 5. K_a reduced energy level diagram for $v_8 = 1$ (dash), $v_{10} = 1$ (dot), and $v_9 = 2$ (solid) states of CH_2═CHF. The energies, reduced by $\bar{B}_0 J(J+1)$ have been calculated from the constants of Tables 5 and 6.

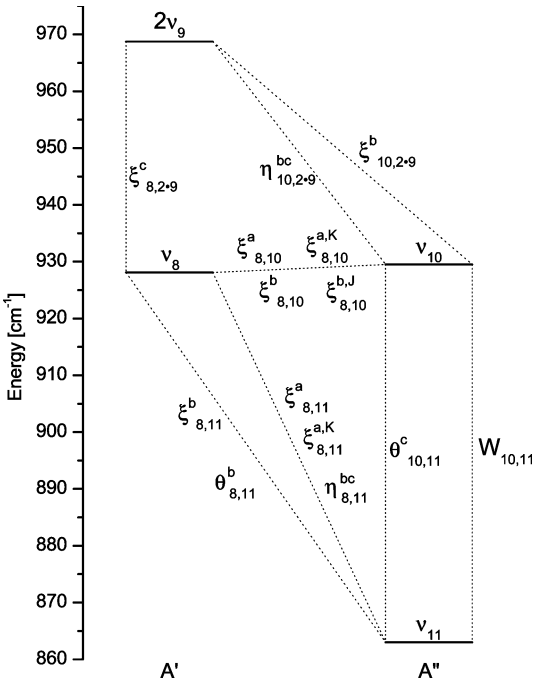

Figure 6. Vibrational energy levels of CH_2═CHF in the region 860−975 cm^{-1}. The scheme of the interaction model adopted is reported: $\xi^{\alpha}_{r,s}$ (α = a, b, or c) denotes first-order Coriolis interaction between v_r and v_s. The anharmonic resonance is denoted by $W_{r,s}$; $\eta^{bc}_{r,s}$ indicates second-order a-type Coriolis interaction ($\Delta K_a = \pm 2$), while $\theta^{b}_{r,s}$ and $\theta^{c}_{r,s}$ indicate b-type and c-type Coriolis interactions, respectively, between levels which differ by $\Delta K_a = \pm 3$.

TABLE 2: Listing of the Observed Crossings in the CH_2=CHF ν_8, ν_{10}, and ν_{11} Vibrations and Type of Resonance[a]

	K_a'				type of resonance	
J'	ν_8	ν_{10}	ν_{11}	$2\nu_9$[b]		
43	0		3^+		b-type Coriolis	$\Delta K_a = \pm 3$
43	1^-		3^+		a-type Coriolis	$\Delta K_a = \pm 2$
7	1^+	1^-			a-type Coriolis	$\Delta K_a = 0$
13	2^+	2^-			a-type Coriolis	$\Delta K_a = 0$
37	3^-			0	c-type Coriolis	$\Delta K_a = \pm 3$
20	3^+	3^-			a-type Coriolis	$\Delta K_a = 0$
42	3^+			2^-	c-type Coriolis	$\Delta K_a = \pm 1$
30		3^+		0	b-type Coriolis	$\Delta K_a = \pm 3$
30		3^+		1^-	a-type Coriolis	$\Delta K_a = \pm 2$
39	4^-			1^+	c-type Coriolis	$\Delta K_a = \pm 3$
25	4^+			1^-	c-type Coriolis	$\Delta K_a = \pm 3$
24		4^-		1^-	b-type Coriolis	$\Delta K_a = \pm 3$
28	4^+	4^-			a-type Coriolis	$\Delta K_a = 0$
19	5^+			2^-	c-type Coriolis	$\Delta K_a = \pm 3$
35		4^+		1^+	b-type Coriolis	$\Delta K_a = \pm 3$
18		5^-		2^-	b-type Coriolis	$\Delta K_a = \pm 3$
36	5^+	5^-			a-type Coriolis	$\Delta K_a = 0$
34		5^+	8^-		c-type Coriolis	$\Delta K_a = \pm 3$
27	$6^\pm$	$6^\mp$			a-type Coriolis	$\Delta K_a = 0$
43	6^-			3^+	c-type Coriolis	$\Delta K_a = \pm 3$
42		6^+		4^-	a-type Coriolis	$\Delta K_a = \pm 2$
38	$7^\pm$	$7^\mp$			a-type Coriolis	$\Delta K_a = 0$
40		7^-		5^+	a-type Coriolis	$\Delta K_a = \pm 2$

[a] The + and − signs associated with K_a' correspond to higher (even) $K_a' + K_c' = J'$ and lower (odd) $K_a' + K_c' = J' + 1$ components of the energy levels, respectively. [b] The K_a' value has been deduced from Figure 5 and the observed crossings in the ν_8 and ν_{10} bands.

order a-type Coriolis resonance. Moreover, in the reduced energy diagram of Figure 5, it is interesting to note the near-resonance of the levels with $K_a' = 4$, 5, and 6 of both ν_8 and ν_{10}; in particular, the $K_a' = 4$ level of ν_8 has lower energy than that corresponding to ν_{10}, while the $K_a' = 6$ level of ν_8 has higher energy than that of ν_{10}. The exchange in the relative position of the levels reflects the observed anomalies in the ^QQ_K clusters of ν_8 and ν_{10} bands previously discussed.

The ν_{11} vibration is perturbed by both ν_8 and ν_{10} states in particular for $K_a' \geq 8$. The ν_{11} and ν_8 fundamentals may interact through a-type as well as b-type Coriolis resonance, while ν_{11} and ν_{10} modes having the same symmetry should interact by c-type Coriolis perturbation and high-order anharmonic resonance. A few observed crossings involving ν_{11} are also included in Table 2. For low K_a' values, high-order perturbations occur, and they affect only a few J values around the crossing. Proceeding toward high K_a' values, the effect of first-order interactions always becomes more important, and for $K_a' \geq 9$, the rovibrational levels of ν_{11} are perturbed for each value of J.

It is worthwhile to note that the occurring interactions also increase the intensity of some transitions of ν_{10} and ν_{11} characterized by $\Delta K_c = \pm 2$. Usually, in the absence of perturbations, these transitions are weak when compared with those having $\Delta K_c = 0$. Furthermore, a number of transitions with $\Delta K_a = \pm 2$, belonging to the ν_8 band, have been identified. It can be noticed that, in the absence of interactions, transitions with $\Delta K_a = \pm 2$ have a negligible intensity and rarely give rise to strong lines. Generally, since the strong Coriolis resonances produce a mixing of the involved rovibrational states, a borrowing of intensity occurs for the weak lines, and transitions with $\Delta K_a = \pm 2$ (a-type), $\Delta K_a = \pm 3$ (b-type), and $\Delta K_c = \pm 2$ (c-type) can be clearly observed.

As previously described, the $2\nu_9$ vibration is also involved in the interaction system, although in the examined spectral range, no transitions belonging to the overtone have been found.

TABLE 3: Matrix Elements of the Perturbation Operators

a-type Coriolis resonance
$\langle J, K\|\mathbf{H}^A\|J, K\rangle = i \cdot[\xi^a + \xi^{a,K}\cdot K^2]\cdot K$
$\langle J, K\|\mathbf{H}^A\|J, K \pm 2\rangle = \mu i/2\cdot\eta^{bc}\cdot F(J, K)\cdot F(J, K \pm 1)$
b-type Coriolis resonance
$\langle J, K\|\mathbf{H}^B\|J, K \pm 1\rangle = i/2\cdot[\xi^b + \xi^{b,J}\cdot J(J+1)]\cdot F(J, K)$
$\langle J, K\|\mathbf{H}^B\|J, K \pm 3\rangle = i/2\cdot\theta^b\cdot F(J, K)\cdot F(J, K \pm 1)\cdot F(J, K \pm 2)$
c-type Coriolis resonance
$\langle J, K\|\mathbf{H}^C\|J, K \pm 1\rangle = \pm 1/2\cdot\xi^c\cdot F(J, K)$
$\langle J, K\|\mathbf{H}^C\|J, K \pm 3\rangle = \pm 1/2\cdot\theta^c\cdot F(J, K)\cdot F(J, K \pm 1)\cdot F(J, K \pm 2)$
high-order anharmonic resonance
$\langle J, K\|\mathbf{H}^{ahn}\|J, K \pm 2\rangle = 1/2\cdot W\cdot F(J, K)\cdot F(J, K \pm 1)$
$F(J, K) = \sqrt{J(J+1) - K(K\pm 1)}$. $\xi^\alpha_{r,s} = \zeta^\alpha_{r,s}\cdot B^\alpha_e\cdot(\omega_r + \omega_s)/(\omega_t\omega_s)^{1/2}$.

The $2\nu_9$, of symmetry species A′, may interact with ν_8 through c-type Coriolis and anharmonic resonances and with ν_{10} through a- and b-type Coriolis perturbations. The $2\nu_9$ vibration considerably complicates the interaction scheme, and many crossings due to high-order perturbations, which mainly interest low K_a' values, have been found in the ν_8 and ν_{10} bands, as reported in Table 2. Proceeding toward high K_a' values, the $2\nu_9$ levels became more close in energy to those of ν_8 and ν_{10}, and for $K_a' \geq 6$, the rovibrational levels of ν_8 and ν_{10} are globally perturbed through first-order Coriolis resonances by the $2\nu_9$ state. Finally, it should be noted that the inclusion of the Fermi resonance between ν_8 and $2\nu_9$ in the least-squares refinement did not produce any improvement, and the related coupling constant could not be reliably determined.

3.3. Simultaneous Fit of ν_8, ν_{10}, and ν_{11}. A simultaneous fit, according to the interaction model reported in Figure 6, is required in order to obtain a suitable set of spectroscopic parameters for the three fundamentals investigated.

The ground and excited rotational energy levels were computed using the Watson's A-reduction Hamiltonian up to the sixth order in the I^r representation

$$\mathbf{H}_v^{rot} = \frac{1}{2}(B+C)\mathbf{P}^2 + \left[A - \frac{1}{2}(B+C)\right]\mathbf{P}_a^2 - \Delta_J\mathbf{P}^4 - \Delta_{JK}\mathbf{P}^2\mathbf{P}_a^2 - \Delta_K\mathbf{P}_a^4 + \Phi_J\mathbf{P}^6 + \Phi_{JK}\mathbf{P}^4\mathbf{P}_a^2 + \Phi_{KJ}\mathbf{P}^2\mathbf{P}_a^4 + \Phi_K\mathbf{P}_a^6 + \left[\frac{1}{2}(B-C) - 2\delta_J\mathbf{P}^2 + 2\phi_J\mathbf{P}^4\right](\mathbf{P}_b^2 - \mathbf{P}_c^2) + [(-\delta_K\mathbf{P}_a^2 + \phi_{JK}\mathbf{P}^2\mathbf{P}_a^2 + \phi_K\mathbf{P}_a^4), (\mathbf{P}_b^2 - \mathbf{P}_c^2)]_+$$

where $\mathbf{P}$ is the operator for the angular momentum and $\mathbf{P}_a$, $\mathbf{P}_b$, and $\mathbf{P}_c$ are its components along the principal inertial axes in the molecular fixed coordinate system, and $[\ ]_+$ is the anticommutator defined as $[X, Y]_+ = XY + YX$.

The ν_8, ν_{10}, and ν_{11} transitions were fitted simultaneously employing the *SPFIT* program written by Pickett,[17] kindly provided to the spectroscopic community by JPL Molecular Spectroscopy. In terms of operators, the Hamiltonian matrix associated with the four vibration systems employed has the following aspect:

	$v_8 = 1$	$v_{10} = 1$	$v_{11} = 1$	$v_9 = 2$
$v_8 = 1$	$\mathbf{H}_{8,8}$	$\mathbf{H}^{A,B}_{8,10}$	$\mathbf{H}^{A,B}_{8,11}$	$\mathbf{H}^{C}_{8,2\cdot9}$
$v_{10} = 1$		$\mathbf{H}_{10,10}$	$\mathbf{H}^{C,Anh}_{10,11}$	$\mathbf{H}^{A,B}_{10,2\cdot9}$
$v_{11} = 1$			$\mathbf{H}_{11,11}$	0
$v_9 = 2$				$\mathbf{H}_{2\cdot9,2\cdot9}$

TABLE 4: Summary of Assignments in the ν_8, ν_{10}, and ν_{11} Bands of CH_2=CHF

	ν_8		ν_{10}		
	a-type component	b-type component	c-type component	pseudo a-type component	ν_{11}
subbranches	^{Q}P, ^{Q}Q, ^{Q}R, ^{S}R	^{P}P, ^{R}P, ^{P}Q, ^{R}Q, ^{P}R, ^{R}R	^{P}P, ^{P}Q, ^{R}Q, ^{R}R	^{O}P, ^{Q}P, ^{O}Q, ^{Q}Q, ^{Q}R	^{P}P, ^{P}Q, ^{R}Q, ^{R}R
assigned transitions	$J' \le 50$, $0 \le K_a' \le 16$	$J' \le 39$, $4 \le K_a' \le 11$	$J' \le 50$, $0 \le K_a' \le 17$	$J' \le 38$, $0 \le K_a' \le 11$	$J' \le 50$, $0 \le K_a' \le 17$
observed asymmetry splitting	$K_a' \le 8$		$K_a' \le 9$		$K_a' \le 8$
number of assigned transitions	3144		3235		3577

TABLE 5: Molecular Constants (cm^{-1}) for ν_8, ν_{10}, ν_{11}, and $2\nu_9$ States of CH_2=CHF

	ground state[a]	ν_8	ν_{10}	ν_{11}	$2\nu_9$
E_v		928.117419(96)[b]	929.486603(84)	863.018189(49)	968.7055(48)
A	2.1543131(4)	2.190790(28)	2.1371708(56)	2.115590(32)	2.148180(50)
B	0.35480820(6)	0.3539404(11)	0.35446577(43)	0.3540522(11)	0.355424(11)
C	0.30414491(5)	0.30334301(40)	0.30437546(34)	0.30435560(39)	0.302289(12)
$\Delta_J \times 10^6$	0.28126(8)	0.28555(17)	0.28340(13)	0.279330(89)	[c]
$\Delta_{JK} \times 10^5$	−0.2537(2)	−0.27608(19)	−0.25048(19)	−0.21845(13)	
$\Delta_K \times 10^4$	0.44367(17)	0.6062(19)	0.43131(11)	0.2721(20)	
$\delta_J \times 10^7$	0.5891(1)	0.6112(12)	0.5786(10)	0.5747(13)	
$\delta_K \times 10^5$	0.1186(1)	0.1675(12)	0.13066(93)	0.07750(64)	
	[d] $\Phi_J \times 10^{12} = 0.47(2)$, $\Phi_{KJ} \times 10^9 = -0.223(8)$, $\Phi_K \times 10^8 = 0.259(14)$, $\phi_J \times 10^{12} = 0.217(5)$, $\phi_K \times 10^9 = 0.46(3)$				
No. of data		3093	3192	3538	
$\sigma \times 10^3$		0.545			

[a] From ref 14. [b] Figures in parentheses are standard deviations in units of the last significant digits. [c] Quartic centrifugal distortion constants fixed to the ground-state value. [d] Ground-state sextic coefficients (ref 14) fixed for the upper levels.

TABLE 6: Interaction Parameters (cm^{-1}) for ν_8, ν_{10}, ν_{11}, and $2\nu_9$ States of CH_2=CHF

$\xi^{a}_{8,10}$	0.357694(12)[a]	$\xi_{8,11}{}^{a}$	0.1620(64)	$\xi^{c}_{8,2\cdot9}$	$0.4468(30) \times 10^{-3}$
$\xi^{a,K}_{8,10}$	$-0.270194(34) \times 10^{-3}$	$\xi^{a,K}_{8,11}$	$-0.10264(59) \times 10^{-3}$		
$\xi^{b}_{8,10}$	0.293753(13)	$\eta^{bc}_{8,11}$	$0.7852(39) \times 10^{-3}$	$W_{10,11}$	$0.2335(25) \times 10^{-3}$
$\xi^{b,J}_{8,10}$	$-0.1328(16) \times 10^{-5}$	$\xi^{b}_{8,11}$	$-0.271(11) \times 10^{-1}$	$\theta^{c}_{10,11}$	$-0.3480(35) \times 10^{-5}$
		$\theta^{bc}_{8,11}$	$-0.2674(49) \times 10^{-5}$		
				$\xi^{b}_{10,2\cdot9}$	$0.22858(22) \times 10^{-1}$
				$\eta^{bc}_{10,2\cdot9}$	$-0.867(25) \times 10^{-4}$

[a] Figures in parentheses are standard deviations in units of the last significant digits.

where

$$\mathbf{H}_{v,v} = \mathrm{E}_v + \mathbf{H}_v^{rot}$$

$$\mathbf{H}^{A,B}_{8,10} = \mathbf{H}^{A}_{8,10} + \mathbf{H}^{B}_{8,10} = i\cdot[\xi^{a}_{8,10}\cdot\mathbf{P}_a + \xi^{a,K}_{8,10}\cdot\mathbf{P}_a{}^3 + \xi^{b}_{8,10}\cdot\mathbf{P}_b + \xi^{b,J}_{8,10}\cdot\mathbf{P}_b\mathbf{P}^2]$$

$$\mathbf{H}^{A,B}_{8,11} = \mathbf{H}^{A}_{8,11} + \mathbf{H}^{B}_{8,11} = i\cdot\xi^{a}_{8,11}\cdot\mathbf{P}_a + \mathrm{i}\cdot\xi^{a,K}_{8,11}\cdot\mathbf{P}_a{}^3 + \eta^{bc}_{8,11}[\mathbf{P}_b, \mathbf{P}_c]_+ + i\cdot\xi^{b}_{8,11}\cdot\mathbf{P}_b + \frac{i}{2}\cdot\theta^{b}_{8,11}(\mathbf{P}_+{}^3 + \mathbf{P}_-{}^3)$$

$$\mathbf{H}^{C}_{8,2\cdot9} = i\cdot\xi^{c}_{8,2\cdot9}\cdot\mathbf{P}_c$$

$$\mathbf{H}^{A,B}_{10,2\cdot9} = \mathbf{H}^{A}_{10,2\cdot9} + \mathbf{H}^{B}_{10,2\cdot9} = \eta^{bc}_{10,2\cdot9}[\mathbf{P}_b, \mathbf{P}_c]_+ + i\cdot\xi^{b}_{10,2\cdot9}\cdot\mathbf{P}_b$$

$$\mathbf{H}^{C,Anh}_{10,11} = \mathbf{H}^{C}_{10,11} + \mathbf{H}^{Anh}_{10,11} = \frac{1}{2}\cdot\theta^{c}_{10,11}(\mathbf{P}_+{}^3 - \mathbf{P}_-{}^3) + W_{10,11}(\mathbf{P}_b{}^2 - \mathbf{P}_c{}^2)$$

and $\mathbf{P}_\pm = \mathbf{P}_b \pm i\cdot\mathbf{P}_c$

The corresponding matrix elements of the perturbation operators are presented in Table 3.

The complete analysis of the ν_8, ν_{10}, and ν_{11} fundamentals led to the assignment of 9956 lines whose details are summarized in Table 4. In the adopted model, a few of the transitions affected by different high-order interactions could not be considered. Therefore, 133 lines were excluded from the final fit.

The upper-state molecular constants for the three fundamentals were determined up to the quartic coefficients using the ground-state parameters fixed at the values given in ref 14 with a standard deviation of 0.545×10^{-3} cm^{-1}. The variation of the sextic distortion terms led to poorly determined values without any significant improvement in the fit. On this basis, the sextic coefficients were constrained to their ground-state values. In addition, the present work led to the determination of the band origin and the rotational constants for the "dark state" $2\nu_9$, and fourteen coupling terms included in the model adopted. The molecular constants and the interaction parameters are listed in Tables 5 and 6, respectively. For completeness, the absolute values of the correlation matrix greater than 80% are reported in Table 7.

Among the quartic centrifugal distortion constants, the Δ_K and δ_K values of ν_8 and ν_{11} deviate almost equivalently but with an opposite sign compared with the corresponding ground-state values. Also, the A rotational constant of the same vibrations shows an analogous trend with a smaller difference compared with the ground-state value. This is due to the strong correlation between the above constants and the first-order a-type Coriolis parameter $\xi^{a}_{8,11}$ which links the ν_8 and ν_{11} vibrations. Attempts made by fixing different parameters to obtain the A and Δ_K values closer to the ground-state ones were unsuccessful. Also, the rotational constants of the $2\nu_9$ "dark state" are strongly correlated, and this is mainly due to the lack of overtone data in the fit. The correlation between the interaction parameters $\xi^{b}_{8,11}$ and $W_{10,11}$ should be explained by considering that some levels of ν_{11} are effected by both types of resonances. Nevertheless, with the complexity of this problem, the strength and the extent of the interactions found taken into account, such behavior was almost expected. Anyway, the constants of Tables 5 and 6

TABLE 7: Absolute Values of the Correlation Matrix Elements a_{ij} of the Final Fit[a]

i	–	j	$\lvert a_{ij}\rvert$%	i	–	j	$\lvert a_{ij}\rvert$ %
$A^{(8)}$	–	$\Delta_K^{(8)}$	99.1	$B^{(11)}$	–	$\xi^{b}_{8,11}$	93.7
$A^{(8)}$	–	$A^{(11)}$	98.7	$\Delta_K^{(11)}$	–	$\xi^{a}_{8,11}$	99.9
$A^{(8)}$	–	$\Delta_K^{(11)}$	98.7	$\Delta_K^{(11)}$	–	$\xi^{a,K}_{8,11}$	97.3
$A^{(8)}$	–	$\eta^{bc}_{8,11}$	96.0	$\Delta_K^{(11)}$	–	$\eta^{bc}_{8,11}$	97.1
$A^{(8)}$	–	$\xi^{a}_{8,11}$	98.6				
$A^{(8)}$	–	$\xi^{a,K}_{8,11}$	95.8	$E_{2\cdot9}$	–	$A^{(2\cdot9)}$	98.2
$B^{(8)}$	–	$W_{10,11}$	84.3	$E_{2\cdot9}$	–	$B^{(2\cdot9)}$	96.5
$B^{(8)}$	–	$\xi^{a}_{8,11}$	98.7	$E_{2\cdot9}$	–	$C^{(2\cdot9)}$	97.1
$B^{(8)}$	–	$\xi^{b}_{8,11}$	86.2	$E_{2\cdot9}$	–	$\xi^{c}_{8,2\cdot9}$	83.8
$\Delta_K^{(8)}$	–	$A^{(11)}$	99.8	$A^{(2\cdot9)}$	–	$B^{(2\cdot9)}$	94.6
$\Delta_K^{(8)}$	–	$\Delta_K^{(11)}$	99.9	$A^{(2\cdot9)}$	–	$C^{(2\cdot9)}$	94.5
$\Delta_K^{(8)}$	–	$\xi^{a}_{8,11}$	99.8	$B^{(2\cdot9)}$	–	$C^{(2\cdot9)}$	99.1
$\Delta_K^{(8)}$	–	$\xi^{a,K}_{8,11}$	96.9	$B^{(2\cdot9)}$	–	$\xi^{c}_{8,2\cdot9}$	84.5
$\Delta_K^{(8)}$	–	$\eta^{bc}_{8,11}$	97.0	$C^{(2\cdot9)}$	–	$\xi^{c}_{8,2\cdot9}$	84.8
$A^{(10)}$	–	$\Delta_K^{(10)}$	85.3	$\xi^{a}_{8,10}$	–	$\xi^{a,K}_{8,10}$	93.9
$A^{(10)}$	–	$\xi^{a,K}_{8,10}$	91.8	$\theta^{b}_{8,11}$	–	$W_{10,11}$	83.6
				$\theta^{b}_{8,11}$	–	$\xi^{b}_{8,11}$	85.2
$A^{(11)}$	–	$\Delta_K^{(11)}$	99.9	$\eta^{bc}_{8,11}$	–	$\xi^{a}_{8,11}$	97.1
$A^{(11)}$	–	$\eta^{bc}_{8,11}$	97.0	$\eta^{bc}_{8,11}$	–	$\xi^{a,K}_{8,11}$	94.7
$A^{(11)}$	–	$\xi^{a}_{8,11}$	99.6	$W_{10,11}$	–	$\xi^{b}_{8,11}$	99.0
$A^{(11)}$	–	$\xi^{a,K}_{8,11}$	97.3	$\xi^{a}_{8,11}$	–	$\xi^{a,K}_{8,11}$	96.1
$B^{(11)}$	–	$W_{10,11}$	93.6				

[a] Only values greater than 80% have been reported.

are obtained with a good standard deviation of the fit and provide the best achieved results.

To reproduce the observed irregularities due to perturbation effects, the predicted spectra using the constants given in Tables 5 and 6 were computed for comparison with the experimental lines in many different regions. The calculated spectra, as can be observed in Figures 2−4, match very well with the observed ones, and the reproduced irregularities confirm the reliability of the perturbation model employed.

As already pointed out, the ν_8 normal mode produces an a/b-hybrid absorption with a predominance of the a-type component. After performing several simulations in selected regions, the a-type component gave results that were twice as strong as the corresponding b-type. Due to the complexity of the interacting system, accurate values of the dipole moment ratio $|\Delta\mu_a/\Delta\mu_b|$ could not be determined.

4. Conclusions

This work deals with the detailed rovibrational analysis of the ν_8, ν_{10}, and ν_{11} absorptions of CH_2═CHF occurring in a spectral region of atmospheric interest; the high-resolution spectra were never previously investigated. Such an analysis of vinyl fluoride is, together with other halogenated ethenes, of high relevance for the atmospheric processes, since photolysis and chemical reactions with ozone, hydroxyl, and nitrate radicals are involved. The three vibrations strongly interact with each other, and in particular, the perturbation effects between ν_8 and ν_{10} are very strong and widespread. Moreover the $2\nu_9$ "dark state" was found to be a perturber mainly involving the ν_8 and ν_{10} vibrations. The interaction mechanisms have been widely understood, and the analysis has led to the assignment of about 10 000 transitions, of which almost all have been simultaneously fitted employing a model with 9 different resonances within the tetrad $\nu_8/\nu_{10}/\nu_{11}/2\nu_9$. The determined spectroscopic parameters should provide opportunities for detailed simulations of atmospheric spectra of this compound, and the knowledge of interactions also make significant contributions relevant to the study of intramolecular vibrational relaxation in vinyl fluoride.

Before closing this section, it is worth commenting about the comparison with the ν_8 (∼721 cm^{-1}), ν_{10} (∼942 cm^{-1}), and ν_{11} (∼896 cm^{-1}) fundamentals of the main isotopologue of vinyl chloride.[18,19] The ν_{10} and ν_{11} vibrations approximately describe similar motions in the two vinyl halides, whereas the ν_8 mode corresponds to the C−Cl stretching in CH_2═CHCl and to the CH_2 rocking in CH_2═CHF. The ν_8 fundamental of vinyl chloride is about 200 cm^{-1} lower than that of vinyl fluoride, and therefore, the involved spectral range of the three fundamentals in the CH_2═CHCl is much wider than that in CH_2═CHF. Not surprisingly, the three vibrations are almost unperturbed in vinyl chloride, while several strong perturbations occur in vinyl fluoride mainly between the ν_8 and ν_{10} motions, since the band origins are almost overlapped.

Acknowledgment. Financial support by MIUR, Rome, is gratefully acknowledged. The authors thank Professor M. Winnewisser for the opportunity to obtain high-resolution infrared spectra on the Giessen instrument some years ago.

References and Notes

(1) Guillory, W. A.; Andrews, G. H. *J. Chem. Phys. A* **1975**, *62*, 4667−4671.
(2) Perry, R. A.; Atkinson, R.; Pitts, J. M., Jr. *J. Chem. Phys.* **1977**, *67*, 458−462.
(3) Vinyl fluoride. Draft report on carcinogens. National toxicolgy program; U. S. Department of Health and Human Services; http://www.mindfully.org/Plastic/Vinyl-Fluoride-Carcinogens-NTP−BOS.htm#crit, 1998.
(4) Sekušak, S.; Liedl, K. R.; Sabliæ, A. *J. Phys. Chem. A* **1998**, *102*, 1583−1594.
(5) Ljubić, J.; Sablić, A. *J. Phys. Chem. A* **2002**, *106*, 4745−4757.
(6) Stoppa, P.; Pietropolli Charmet, A.; Visinoni, R.; Giorgianni, S. *Mol. Phys.* **2005**, *103*, 657−666.
(7) Scherer, J. R.; Potts, W. J. *J. Chem. Phys.* **1959**, *31*, 1691−1692.
(8) McKean, D. C. *Spectrochim. Acta* **1975**, *31A*, 1167−1186.
(9) Torkington, P.; Thompson, H. W. *Trans. Faraday Soc.* **1945**, *41*, 236−245.
(10) Bak, B.; Christensen, D. *Spectrochim. Acta* **1958**, *12*, 355−369.
(11) Elst, R.; Oskam, A. *J. Mol. Spectrosc.* **1971**, *39*, 357−363.
(12) Gerry, M. L. C. *J. Mol. Spectrosc.* **1973**, *45*, 71−78.
(13) Hayashi, M.; Inagusa, T. *J. Mol. Spectrosc.* **1989**, *138*, 135−140.
(14) Stoppa, P.; Giorgianni, S.; Gambi, A.; De Lorenzi, A.; Ghersetti, S. *Mol. Phys.* **1995**, *84*, 281−290.
(15) Plummer, G. M.; Winnewisser, G.; Winnewisser, M.; Hahn, J.; Reinartz, K. *J. Mol. Spectrosc.* **1987**, *126*, 255−269.
(16) Guelachvili, G.; Narahari, R. K. *Handbook of Infrared Standards*; Academic Press: New York, 1986.
(17) Pickett, H. M. *J. Mol. Spectrosc.* **1991**, *148*, 371−377.
(18) De Lorenzi, A.; Giorgianni, S.; Bini, R. *Mol. Phys.* **1999**, *96*, 101−108.
(19) De Lorenzi, A.; Giorgianni, S.; Bini, R. *Mol. Phys.* **2000**, *98*, 355−362.